Physical properties of the R3Pt23Si11 compounds with volatile rare earth: Sm, Eu, Tm and Yb

Christine Opagiste, Camille Barbier, Richard Heattel, Rose-Marie Galéra

Physical properties of the $R_3Pt_{23}Si_{11}$ compounds with volatile rare earth: Sm, Eu, Tm and Yb

C. Opagiste[a,b,1], C. Barbier[b,a], R. Haettel[b,a], R. M. Galéra[b,a]

[a] *Univ.Grenoble Alpes, Inst NEEL, F-38042 Grenoble, France*
[b] *CNRS,Inst NEEL, F-38042 Grenoble, France*

Abstract

The new $R_3Pt_{23}Si_{11}$ series, where R is a rare earth, has been completed with the synthesis of three new compounds with volatile rare earth : R = Eu, Sm, and Tm. The studies of their physical properties have been performed along with those of the $Yb_3Pt_{23}Si_{11}$ compound. The X-ray powder diffraction patterns confirm that they all crystallize in the same face-centered cubic structure, space group $Fm\bar{3}m$, as the rest of the series. The refinements of the diffraction patterns show an anomalously high lattice parameter in $Eu_3Pt_{23}Si_{11}$ and $Yb_3Pt_{23}Si_{11}$, indicating a divalent valence state for Eu and Yb. This 2+ valence state for Eu and Yb ions is confirmed by the magnetic measurements. A ferromagnetic order is observed at $T_C = 5.54\pm0.07$ K and 10.12 ± 0.07 K in $Eu_3Pt_{23}Si_{11}$ and $Sm_3Pt_{23}Si_{11}$ respectively. In $Tm_3Pt_{23}Si_{11}$ no magnetic order is found down to 0.36 K while $Yb_3Pt_{23}Si_{11}$ reveals a diamagnetic behavior. At low temperatures the spontaneous moment, M_s, in $Eu_3Pt_{23}Si_{11}$ is in agreement with a L=0, S=7/2 state for the Eu^{2+} ion. On the contrary in $Sm_3Pt_{23}Si_{11}$, M_s is far below the 0.714 μ_B expected for the saturated moment of the Sm^{3+} in the J=7/2 ground state multiplet.

Keywords: rare-earth intermetallics ferromagnetism Van Vleck paramagnetism diamagnetism heat-capacity

1. Introduction

We recently undertook the investigation of the new series $R_3Pt_{23}Si_{11}$ where R is a rare earth element. The existence of the defined compounds

[1] christine.opagiste@grenoble.cnrs.fr

$Ce_3Pt_{23}Si_{11}$ was first reported by Tursina et al [1]. $Ce_3Pt_{23}Si_{11}$ crystallizes in a face-centered cubic crystal structure belonging to the $Fm\bar{3}m$ space group. Studies on a very high quality single crystal of $Ce_3Pt_{23}Si_{11}$ have revealed that it orders ferromagnetically at T_C=0.44 K [2, 3]. Thereafter we have continued the synthesis and the study of the physical properties of new compounds in this series with all the nonvolatile rare earth elements. High quality polycrystalline samples have been successfully synthesized with R=Pr, Nd, Gd, Tb, Dy, Ho and Er [4, 5, 6]. All the compounds with heavy rare earths present a ferromagnetic ordering. The Curie temperatures range between 42 K and 3.4 K for $Gd_3Pt_{23}Si_{11}$ and $Er_3Pt_{23}Si_{11}$ respectively. They are in full consistency with the de Gennes law [7]. At low temperatures, $Pr_3Pt_{23}Si_{11}$ becomes a Van Vleck paramagnet due to a non-magnetic crystalline electric field (CEF) ground state while $Nd_3Pt_{23}Si_{11}$ orders antiferromagnetically at T_N=1.6 K. In the paramagnetic phase, the magnetic susceptibility of all these compounds follows a Curie-Weiss law, as expected for normal trivalent rare earth ions. Up to present the only compound in the series, synthesized with a volatile rare earth was $Yb_3Pt_{23}Si_{11}$ [8]. It was reported as a moderately enhanced paramagnetic compound with fairly unstable $4f$ electronic shell. In the literature compounds with Sm and Eu, two other volatile rare earths, are fairly often reported to exhibit anomalous magnetic properties, such as heavy fermion or mixed valence behaviors [9, 10, 11, 12]. Therefore we undertook to complete the $R_3Pt_{23}Si_{11}$ series with the synthesis of the new compounds; $Sm_3Pt_{23}Si_{11}$, $Eu_3Pt_{23}Si_{11}$ and $Tm_3Pt_{23}Si_{11}$. We present here a first study of the crystallographic and physical properties of these newly synthesized compounds. To get a further insight into the magnetic properties of $Yb_3Pt_{23}Si_{11}$ we have also synthesized and studied this compound.

2. Sample synthesis and crystallographic studies

The polycrystalline samples of $Sm_3Pt_{23}Si_{11}$, $Eu_3Pt_{23}Si_{11}$, $Tm_3Pt_{23}Si_{11}$, and $Yb_3Pt_{23}Si_{11}$, have been prepared by the conventional induction melting technique in a water-cooled copper crucible under a highly purified argon atmosphere. The Pt and Si were purchased from Alfa Aesar with a purity greater than 99.95% and the rare earth elements from Johnson Matthey with a purity of 99.9%. They all present a high saturating vapor pressure at the Pt melting temperature. To limit their evaporation losses during the melt, a two steps synthesis process was used. The intermediate binary alloy $Pt_{23}Si_{11}$ was prepared first by melting Pt and Si in stoechiometric amounts. This

allows reducing the melt temperature from 1769 °C to about 1100 °C [13]. The rare earth element was added in a second step. A slight evaporation of the rare earth element (0.6 to 1.5%) can nonetheless be observed. When it is the case, this was systematically compensated by a further addition of the rare earth element in order to obtain the nominal stoichiometry 3:23:11 for R:Pt:Si. Finally the samples were melted several times to improve their homogeneity. Mass losses during this last step were negligible. No further heat treatment was applied except for the $Tm_3Pt_{23}Si_{11}$ compound, which was annealed over 5 days at 850 °C under a pressure of 10^{-8} mbar.

The crystal structure and the sample quality were checked by powder X-ray diffraction on a Philips PW1730 diffractometer using the Cu-K_α radiation. The refinements of the X-ray diffraction patterns were performed using the FullProf program [14]. For all compounds the results of the refinements are fully consistent with the face-centered cubic crystal structure (space group $Fm\bar{3}m$) reported for the first time by Tursina *et al.* [1] for the $Ce_3Pt_{23}Si_{11}$ compound. For instance the figure 1 shows the experimental and simulated X-ray diffraction patterns for $Eu_3Pt_{23}Si_{11}$. Within the experimental resolution of the conventional powder X-ray diffraction technique used here, no impurity phases are detected in $Sm_3Pt_{23}Si_{11}$, $Eu_3Pt_{23}Si_{11}$ and $Yb_3Pt_{23}Si_{11}$. In $Tm_3Pt_{23}Si_{11}$ traces of the Pt_2Si and $Tm_6Pt_{30}Si_{19}$ phases (less than 5%) are observed.

Scanning electron microscopy (SEM) analyses performed on these compounds, reveal a good homogeneity of the polycrystalline samples. Some weak traces of $Pt_{12}Si_5$ and Pt_3Si are observed in the grain boundaries. Seeking further, submicrometric traces of a R-Pt-Si ternary phase have been observed in a much smaller amount in the Sm and Yb based compounds. These traces being submicrometric it is not possible to determine unambiguously their stoechiometry.

The refined lattice parameters at room temperature for the four compounds are reported in table 1 together with several details of the Rietveld refinements. The atomic coordinates in the elementary cell are summarized in tables 2 to 5 for each compound. Figure 2 shows the evolution of the lattice parameter within the $R_3Pt_{23}Si_{11}$ series. Except for the Eu and Yb compounds, the decrease of the lattice parameter with increasing rare earth atomic number is consistent with the lanthanide contraction effect as illustrated by the evolution of trivalent ionic radii. The cell parameter values of $Eu_3Pt_{23}Si_{11}$ and $Yb_3Pt_{23}Si_{11}$ are clearly above this curve, indicating that the valence of these rare earths is very probably two.

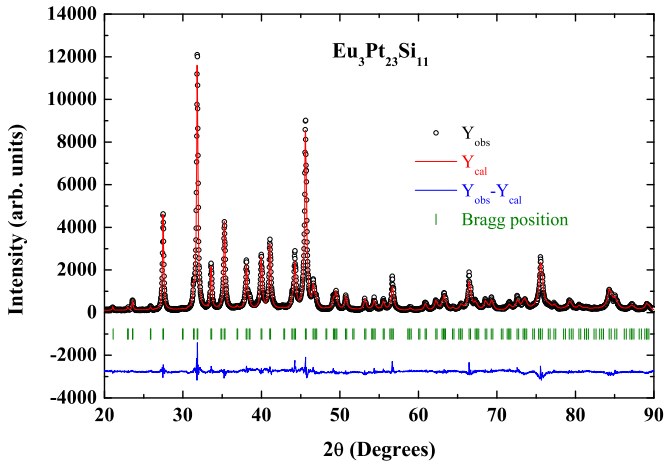

Figure 1: (Color online) Powder X-ray diffraction pattern of $Eu_3Pt_{23}Si_{11}$ compared with the FullProf refinement for the fcc $Ce_3Pt_{23}Si_{11}$-type structure (space group $Fm\bar{3}m$).

Table 1: Crystallographic details and results of the FullProf refinements realized assuming the face-centered cubic $Ce_3Pt_{23}Si_{11}$-type crystal structure: space group $Fm\bar{3}m$ (n^o 225) and Z=8. Column 4 gives the number of measured reflections. For all compounds the same 28 parameters are refined. * Traces of the Pt_2Si and $Tm_6Pt_{30}Si_{19}$ phases ($\leq 5\%$).

Compound	a(Å)	D_{cal} (g/cm^3)	Reflexions	χ^2
$Sm_3Pt_{23}Si_{11}$	16.8370(8)	14.605	293	5.91
$Eu_3Pt_{23}Si_{11}$	16.8691(6)	14.534	278	5.95
$Tm_3Pt_{23}Si_{11}$*	16.794(2)	14.873	310	5.51
$Yb_3Pt_{23}Si_{11}$	16.8164(7)	14.848	276	5.63

Table 2: Atomic coordinates and isotropic displacement parameters for $Sm_3Pt_{23}Si_{11}$.

Atom	Wyckoff site	x/a	y/b	z/c	U_{iso} (Å^2)	Occupation
Sm	24*d*	0	1/4	1/4	1.0	1
Pt_1	32*f*	0.0826(2)	0.0826(2)	0.0826(2)	1.4	1
Pt_2	32*f*	0.3080(1)	0.3080(1)	0.3080(1)	1.1	1
Pt_3	24*e*	0.3746(3)	0	0	0.7	1
Pt_4	96*k*	0.0849(1)	0.0849(1)	0.2523(2)	1.5	1
Si_1	24*e*	0.180(2)	0	0	1.5	1
Si_2	32*f*	0.1723(8)	0.1723(8)	0.1723(8)	1.5	1
Si_3	32*f*	0.3926(8)	0.3926(8)	0.3926(8)	1.5	1

Table 3: Atomic coordinates and isotropic displacement parameters for $Eu_3Pt_{23}Si_{11}$.

Atom	Wyckoff site	x/a	y/b	z/c	U_{iso} (Å^2)	Occupation
Eu	24*d*	0	1/4	1/4	1.2	1
Pt_1	32*f*	0.0835(2)	0.0835(2)	0.0835(2)	1.2	1
Pt_2	32*f*	0.3081(1)	0.3081(1)	0.3081(1)	0.6	1
Pt_3	24*e*	0.3764(2)	0	0	1.4	1
Pt_4	96*k*	0.0845(1)	0.0845(1)	0.2532(2)	1.1	1
Si_1	24*e*	0.187(2)	0	0	1.7	1
Si_2	32*f*	0.1693(7)	0.1693(7)	0.1693(7)	1.7	1
Si_3	32*f*	0.3880(7)	0.3880(7)	0.3880(7)	1.7	1

Table 4: Atomic coordinates and isotropic displacement parameters for $Tm_3Pt_{23}Si_{11}$.

Atom	Wyckoff site	x/a	y/b	z/c	U_{iso} (Å^2)	Occupation
Tm	24*d*	0	1/4	1/4	1.2	1
Pt_1	32*f*	0.0818(2)	0.0818(2)	0.0818(2)	1.2	1
Pt_2	32*f*	0.3093(2)	0.3093(2)	0.3093(2)	0.6	1
Pt_3	24*e*	0.3753(5)	0	0	1.4	1
Pt_4	96*k*	0.0853(2)	0.0853(2)	0.2558(3)	1.1	1
Si_1	24*e*	0.189(3)	0	0	1.7	1
Si_2	32*f*	0.177(1)	0.177(1)	0.177(1)	1.7	1
Si_3	32*f*	0.384(1)	0.384(1)	0.384(1)	1.7	1

Table 5: Atomic coordinates and isotropic displacement parameters for $Yb_3Pt_{23}Si_{11}$.

Atom	Wyckoff site	x/a	y/b	z/c	U_{iso} (Å^2)	Occupation
Yb	24*d*	0	1/4	1/4	0.8	1
Pt_1	32*f*	0.0825(2)	0.0825(2)	0.0825(2)	1.4	1
Pt_2	32*f*	0.3087(1)	0.3087(1)	0.3087(1)	1.4	1
Pt_3	24*e*	0.3752(3)	0	0	0.4	1
Pt_4	96*k*	0.0853(1)	0.0853(1)	0.2533(1)	1.2	1
Si_1	24*e*	0.187(2)	0	0	1.5	1
Si_2	32*f*	0.1717(8)	0.1717(8)	0.1717(8)	1.5	1
Si_3	32*f*	0.3896(8)	0.3896(8)	0.3896(8)	1.5	1

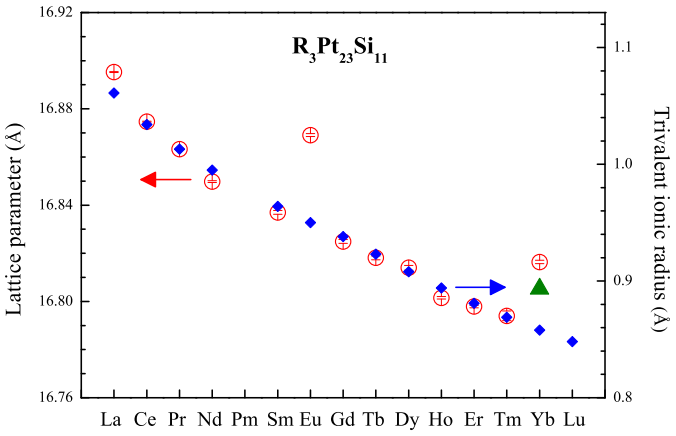

Figure 2: (Color online) Evolution of the lattice parameter in the fcc $R_3Pt_{23}Si_{11}$ series. Dots represent the data from the present work and from Ref. [6], while the triangle gives the lattice parameter given in Ref. [8] for $Yb_3Pt_{23}Si_{11}$. This evolution is compared with the ionic radius evolution of the trivalent rare earth ions (diamonds).

3. Magnetic and thermodynamic properties

Magnetic measurements were performed on polycrystalline samples in the temperature range 1.9 K-300 K. They are based on the extraction technique. They were performed in fields up to 5 T using a Quantum Design MPMS magnetometer (resolution 2×10^{-11} Am^2) and in fields up to 10 T using a non-commercial experimental set-up equipped with resistive detection coils (resolution 5×10^{-7} Am^2). Two type of measurements have been performed; the thermal variation of the magnetization under an applied field of 0.01 T and the field variation of the isothermal magnetization. In this second case the same procedure has been followed at each temperature. Starting from the demagnetized state the field is increased up to its maximum value and then decreased down to zero. This allows to measure the first magnetization curve and to check the remanence. For all the studied compounds no remanent magnetization was observed. Both, the inverse paramagnetic susceptibility and the spontaneous magnetization in the ferromagnetic phase were deduced from the Arrott plots [15]: $M^2 = f(H/M)$. Figure 3 illustrates this determination for $Eu_3Pt_{23}Si_{11}$.

The heat capacity was measured using the relaxation method with a commercial Quantum Design PPMS. The measurements were focused at low temperatures in order to determine precisely the temperature of the magnetic transitions.

3.1. $Sm_3Pt_{23}Si_{11}$

Figure 4 (a) shows the thermal evolution of the inverse magnetic susceptibility of $Sm_3Pt_{23}Si_{11}$. In the temperature range 100 K-300 K it increases apparently linearly with the temperature, however the experimental slope is three times smaller than the expected one for paramagnetic Sm^{3+} ions. Below 100 K, $1/\chi$ shows a downward curvature and tends to zero around 10 K. The thermal variations at low temperatures of the heat capacity and the magnetic moment in an applied field of 0.01 T are reported in figure 4 (b). At 10 K, a lambda anomaly is observed in the heat capacity curve (Note that the very small bump around 5 K is very likely due to the Sm-Pt-Si impurity phases detected by SEM observations). At the same temperature the M(0.01 T) curve shows a steep increase. This confirms that the transition is of magnetic origin and of ferromagnetic-type consistently with the first magnetization curves reported in figure 4 (c). The Curie temperature was deduced at the inflexion point of the lambda-type anomaly of the specific

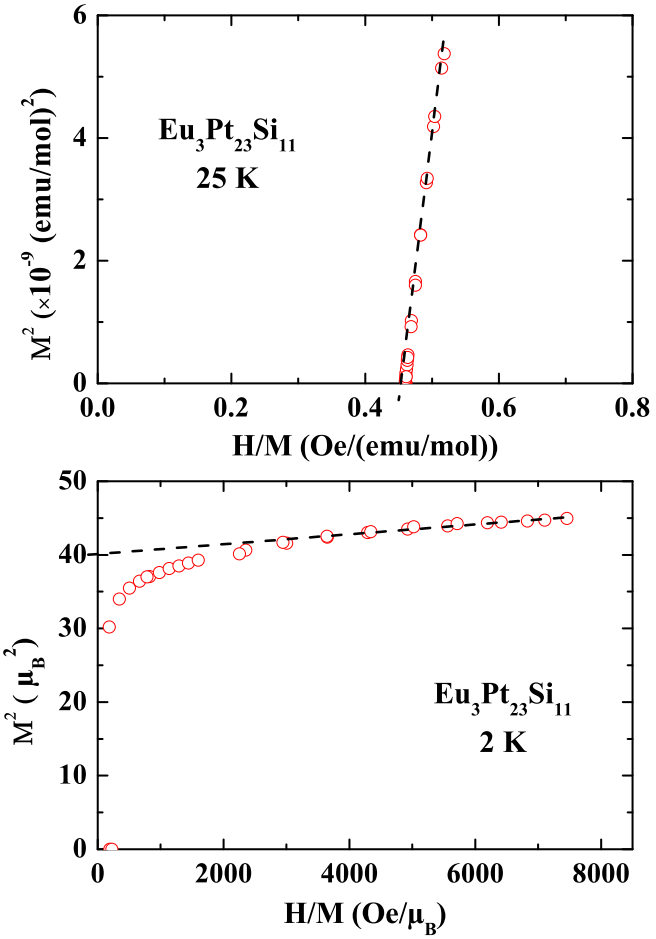

Figure 3: (Color online) (upper part): in the paramagnetic phase the inverse susceptibility is obtained at the interception of the H/M axis and the linear part of the curve $M^2 = f(H/M)$, (lower part): in the ferromagnetic phase, the spontaneous magnetization is evaluated at the interception of the M^2 axis and the linear part of the curve $M^2 = f(H/M)$.

heat curve, T_C=10.12±0.06 K. The thermal variation of the spontaneous magnetization, M_s, deduced from the magnetization curves is reported in figure 4 (d). At 2 K, M_s=0.21 μ_B/Sm. Its extrapolation at T=0 K reaches ≈0.22 μ_B. This value much smaller than the M_s(0 K)=0.714 μ_B expected for the free Sm^{3+} ion, is comparable to those reported previously in several ferromagnetic samarium compounds [16]. As for the other rare earths the reduction of the moment is due to the crystalline electric field (CEF) effects. But in the case of Sm^{3+} ions, because the two first excited, J=7/2 and J=9/2, multiplets are relatively close in energy to the fundamental J=5/2 multiplet [17], it is necessary to account for the CEF effects, not only on the fundamental, but also on these excited multiplets. The mixing of these higher multiplets into the fundamental leads to a stronger reduction of the magnetic moment [16, 18]. In the paramagnetic range the consequence of this mixing is a magnetic susceptibility, which is the sum of a Curie-type term, inversely proportional to the temperature, and a Van Vleck-type term, independent of the temperature. According to that, the line in figure 4 (a) is a rough fit using the modified Curie-Weiss law $\chi = \chi_0 + C/(T - \theta_p)$ with χ_0=4.5×10^{-4} emu/mol, the constant Van Vleck susceptibility, C=0.089 emu/mol the theoretical value of the Sm^{3+} Curie constant within the fundamental multiplet and θ_p=10 K, the paramagnetic Curie temperature (note that here θ_p=T_C).

3.2. $Eu_3Pt_{23}Si_{11}$

Figure 5 (a) shows the thermal evolution of the inverse magnetic susceptibility of $Eu_3Pt_{23}Si_{11}$ deduced from the thermal dependence of the magnetic moment under 0.01 T and from the Arrott plots of the magnetization curves. Both determinations are fully consistent. The experimental inverse susceptibility increases linearly with the temperature. It is compared in the same figure to the theoretical Curie-Weiss-type behavior expected for an Eu^{2+} ion: $1/\chi$=T/C-n_{ex}, with C=7.875 emu/mol, the Curie constant of the Eu^{2+} ion, and n_{ex}=0.9 $(emu/mol)^{-1}$, the exchange coefficient. The experimental slope is slightly larger that the theoretical one, this discrepancy is ascribed to the diamagnetic contribution of the matrix, as observed on $La_3Pt_{23}Si_{11}$. In Figure 5 (b) are reported the thermal variation of the heat capacity and the magnetic moment, M(0.01 T) in the low temperature region. Below 7 K, M(0.01 T) rises steeply and concomitantly the specific heat shows a lambda anomaly. This, together with the magnetization processes, shown in figure 5 (c), is consistent with a ferromagnetic transition at T_C=5.54±0.07 K. The spontaneous magnetization, M_s, deduced from the magnetization curves

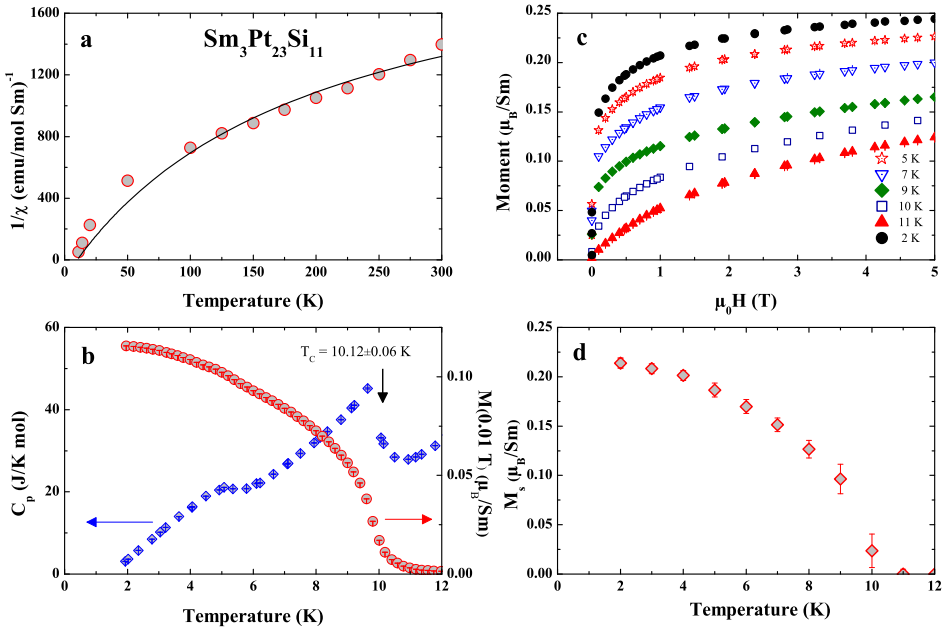

Figure 4: (Color online) $Sm_3Pt_{23}Si_{11}$: (a) thermal evolution of the inverse magnetic susceptibility. The dots represent the experimental data and the line a modified Curie-Weiss law $\chi = \chi_0 + C/(T - \theta_p)$ as explained in the text. (b) comparison between the thermal variation of the magnetic moment under an applied field of 0.01 T (dots) and thermal evolution of the specific heat (diamonds) in the low temperature range, (c) isothermal first magnetization curves measured up to 5 T in the temperature range 2 K-11 K. (d) Thermal variation of the spontaneous magnetization, M_s, deduced from the Arrott plots.

is reported in figure 5 (d). At 2 K, M_s reaches 6.3±0.20 μ_B/Eu. The extrapolation of the curve at T=0 K gives M_s(0 K)≈6.5 μ_B, in agreement with the expected value of 7 μ_B for the S=7/2 state of the Eu^{2+} ion. This is fully consistent with the value of the lattice parameter (see figure 2).

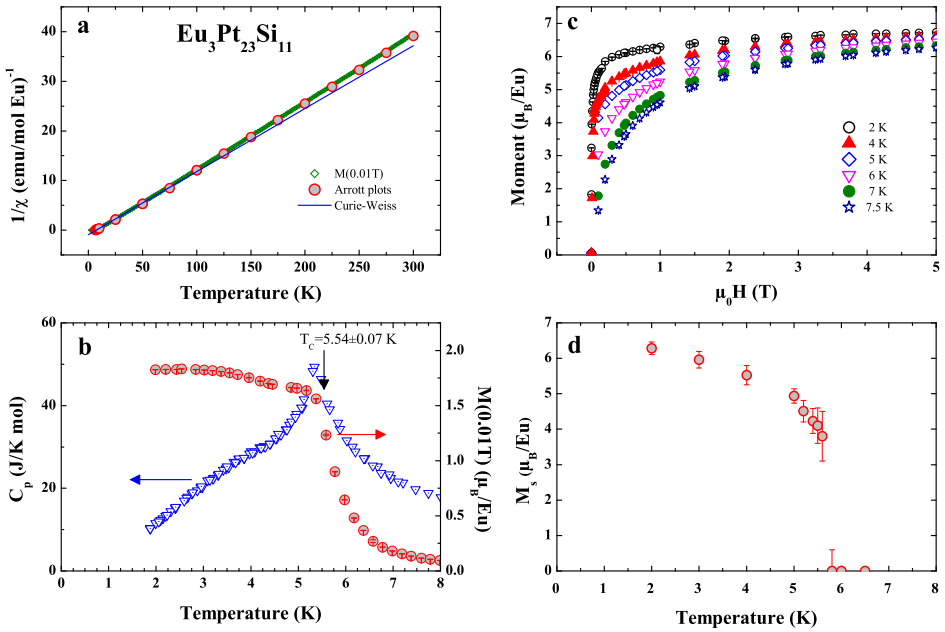

Figure 5: (Color online) $Eu_3Pt_{23}Si_{11}$: (a) thermal evolution of the inverse magnetic susceptibility determined from the thermal dependence of the magnetic moment under 0.01 T (open diamonds) and from the Arrott plots of the magnetization curves (open dots). The line corresponds the Curie-Weiss law for an Eu^{2+} ion and an exchange coefficient n_{ex}=0.9 emu/mol Eu. (b) comparison between the thermal variation of M(0.01 T) (dots) and of the specific heat (triangles). The Curie temperature T_C is deduced from the inflexion point of the lambda anomaly. (c) isothermal first magnetization curves measured up to 5 T in the temperature range 2 K-7.5 K. (d) Thermal variation of the spontaneous magnetization, M_s, deduced from the Arrott plots.

3.3. $Tm_3Pt_{23}Si_{11}$

Figure 6 (a) shows that the inverse magnetic susceptibility of $Tm_3Pt_{23}Si_{11}$ follows a Curie-Weiss law in the whole explored temperature range. The

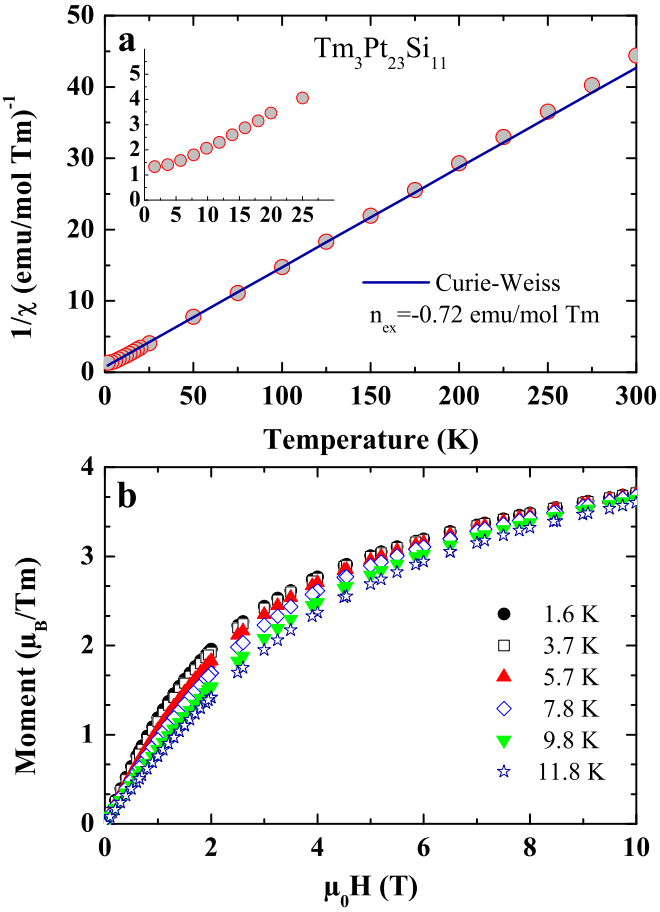

Figure 6: (Color online) a) Thermal dependence of the inverse magnetic susceptibility in $Tm_3Pt_{23}Si_{11}$. The dots represent the experimental data deduced from the Arrott plots of the magnetization curves and the line the calculated data from the Curie-Weiss law: $1/\chi$=(T/C)-n_{ex}, with n_{ex}=-0.72 (emu/mol)$^{-1}$, the exchange coefficient. The inset emphasizes the behavior at low temperature of $1/\chi$. b) Magnetization curves measured in fields up to 10 T at low temperatures.

data are well fitted using the theoretical Curie constant of the Tm^{3+} ion, C=7.146 emu/mol and a negative exchange coefficient, n_{ex}=-0.72 $(emu/mol)^{-1}$, that let suppose the existence of antiferromagnetic correlations. Down to the base temperature the magnetization curves confirm that the compound remains paramagnetic (see Fig. 6 (b)). In this low temperature region the inverse susceptibility seems to tend to a constant value. The Tm^{3+} ion is a non-Kramers ion therefore the CEF lifting of the degeneracy of the ground multiplet, J=6, may select a non-magnetic CEF ground state, hence leading to a Van Vleck behaviour of the susceptibility when decreasing the temperature. In order to seek for an eventual transition, specific heat measurements have been performed down to 0.36 K. No transition could be observed.

3.4. $Yb_3Pt_{23}Si_{11}$

While for the Sm, Eu or Tm compounds masses larger than few tens of mg saturate the detection of the magnetometers, for $Yb_3Pt_{23}Si_{11}$ it is necessary to use a large mass to measure accurately the magnetic signal. Figure 7 shows the magnetization of a mass of 294 mg of $Yb_3Pt_{23}Si_{11}$, measured on the Quantum Design MPMS magnetometer. One observes that the low temperature paramagnetic signal decreases rapidly as temperature is raised. At 100 K the magnetization becomes negative and decreases linearly with the applied field. Warming up the sample, the slope continues to decreases up and stabilizes around 200 K. Above 200 K the slope of the magnetization becomes temperature independent. This is characteristic of a diamagnetic behavior. Many Yb compounds exhibit anomalous magnetic behavior resulting from an intermediate valence state of the Yb ions between 2+ and 3+ [11, 12]. The fact that $Yb_3Pt_{23}Si_{11}$ is diamagnetic and the high value of its lattice parameter, as noticed previously, are strong evidence of a divalent state of the Yb ions. In this case the $4f$ shell is full and non-magnetic, exactly as the non-magnetic $La_3Pt_{23}Si_{11}$ compound. The diamagnetic behavior observed in both the Yb and the La compounds is thus consistent with a diamagnetic signal of the matrix in the $R_3Pt_{23}Si_{11}$ series. According to that the paramagnetic signal observed at low temperatures is ascribed to the existence of a Yb^{3+} impurity phase. The magnetic susceptibility of this impurity has been deduced from the low temperature magnetizations curves (see figure 8). From the slope of the inverse susceptibility it is estimated that the sample contains $\approx$0.05 weight percent of Yb^{3+} ions. As mentioned before in SEM observations, traces of unidentified impurity phases have been found. However specific heat measurements let suppose that very certainly this im-

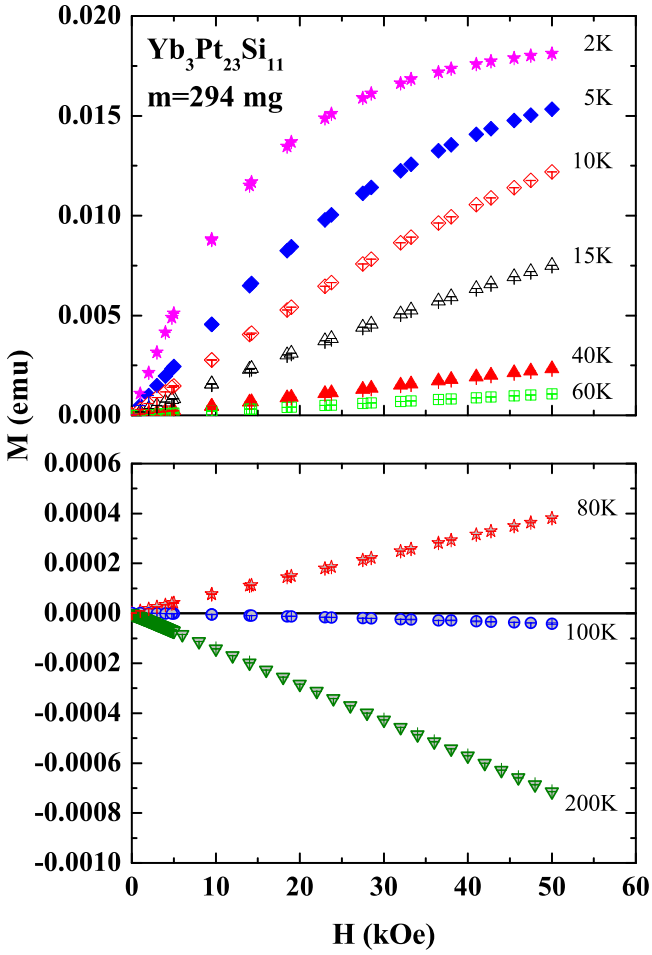

Figure 7: (Color online) Magnetization curves measured on a mass of 294 mg of the $Yb_3Pt_{23}Si_{11}$.

purity phase orders magnetically at very low temperature. In figure 9, the C_p/T curves of La-, Ce- and $Yb_3Pt_{23}Si_{11}$ are compared. Plotting Cp/T *vs* T emphasized any anomaly at very low temperature. It can be observed that the C_p/T curve of $Yb_3Pt_{23}Si_{11}$ tends to increase at the lowest temperatures. Again it is worth noting that the impurity concentration is vanishingly small because this feature is not directly observed on the C_p curve.

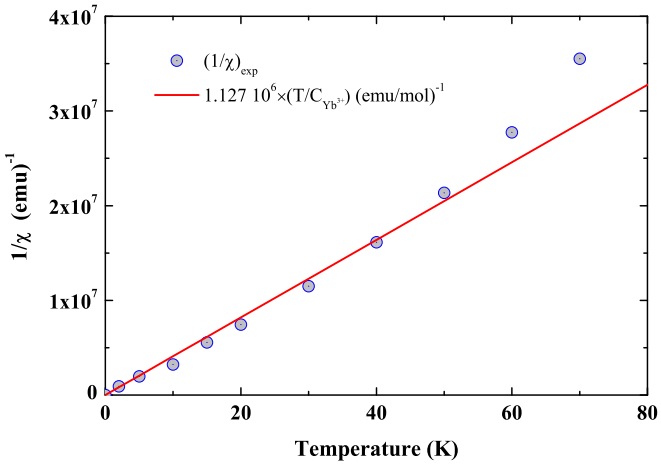

Figure 8: (Color online) Inverse susceptibility of the impurity Yb-Pt-Si phase in the $Yb_3Pt_{23}Si_{11}$ compound, deduced from the Arrott's plots under 70 K. The line represents the calculated inverse susceptibility assuming a Curie law ($C_{Yb^{3+}}$=2.751 emu/mol) for the Yb ions in the impurity phase.

4. Discussion

Figure 10 compares the evolution of the ordering temperatures, in the whole $R_3Pt_{23}Si_{11}$ series, with the de Gennes factors. For all trivalent ions a very good agreement is observed between theoretical expectations and experimental values. This confirms that in the series the interactions between magnetic ions are mediated by indirect RKKY interactions. The discrepancy in figure 10 between the Curie temperature of the Eu compound and the de Gennes factor is due to the divalent state of the Eu ions. In the series the interactions are mostly of ferromagnetic type excepted in $Nd_3Pt_{23}Si_{11}$

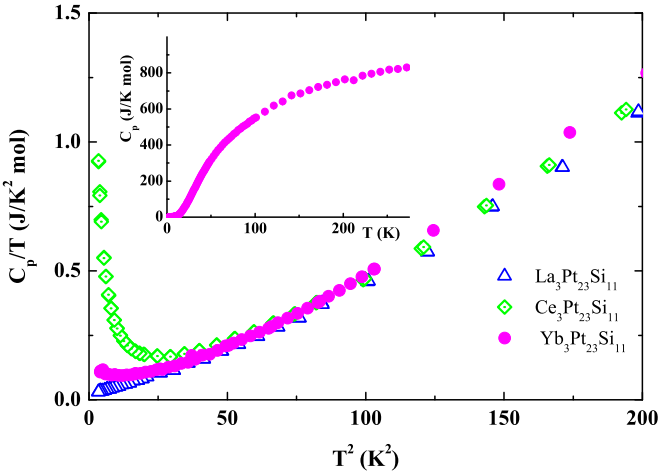

Figure 9: (Color online) Comparison between the experimental C_p/T curves of $La_3Pt_{23}Si_{11}$, $Ce_3Pt_{23}Si_{11}$ and $Yb_3Pt_{23}Si_{11}$. The inset shows the specific heat of $Yb_3Pt_{23}Si_{11}$.

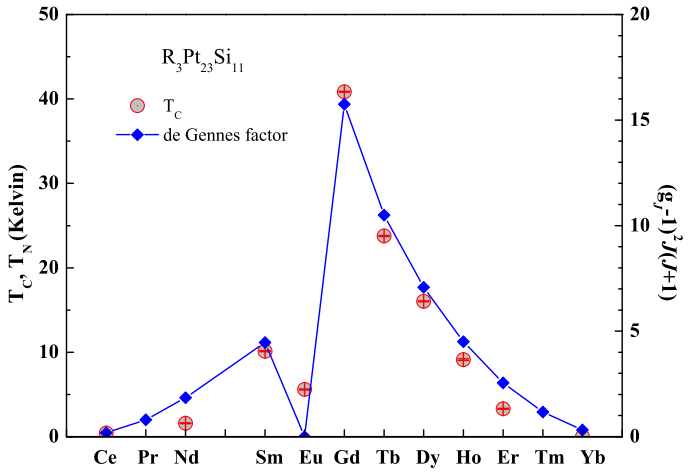

Figure 10: (Color online) Comparison between the experimental ordering temperatures and the de Gennes factor in the whole $R_3Pt_{23}Si_{11}$ series. The Pr and Tm compounds, where the rare earth ion is trivalent, behave as Van Vleck paramagnets at low temperatures. In the Eu and Yb compounds the rare earth are divalent.

where an antiferromagnetic phase transition is observed at 1.6 K [5] and in $Tm_3Pt_{23}Si_{11}$ where negative values of θ_p suggest antiferromagnetic correlations in the paramagnetic phase. Except for the Gd and Eu compounds, for which the rare earth ion is in a S state, the splitting of the J multiplet by the CEF interactions give rise to a reduction of the magnetic moment at low temperature for all the compounds. In $Pr_3Pt_{23}Si_{11}$ and $Tm_3Pt_{23}Si_{11}$ they stabilize a non-magnetic ground state leading to a Van Vleck paramagnetic behaviour. In the paramagnetic phase all the compounds follow the Curie-Weiss law except $Sm_3Pt_{23}Si_{11}$.

We have shown that in $Yb_3Pt_{23}Si_{11}$ the Yb ions are divalent and therefore non-magnetic. The diamagnetic susceptibility deduced for this compound is χ_{dia}=-2.6$\times 10^{-4}$ emu/mol. Its absolute value is one order of magnitude larger than that of $La_3Pt_{23}Si_{11}$ (χ_{dia}=-4.5$\times 10^{-5}$ emu/mol).

5. Conclusion

The present study shows that compounds of the $R_3Pt_{23}Si_{11}$ series can be synthesized within the same crystallographic structure with almost all the rare earth ions (as it does not present interest for the magnetism, the Lu compound has not been synthesized). Our crystallographic and magnetic results allow concluding that the Eu and Yb ions are divalent in this structure. The $Sm_3Pt_{23}Si_{11}$ compound follows a modified Curie-Weiss law due to the mixing of the excited multiplets and orders ferromagnetically at 10.2 K. $Eu_3Pt_{23}Si_{11}$ orders also ferromagnetically at 5.54 K, its magnetic moment is fully consistent with a S=7/2 state. No order is found down to 0.36 K for $Tm_3Pt_{23}Si_{11}$ confirming a non-magnetic CEF ground state. The $Yb_3Pt_{23}Si_{11}$ compound presents a diamagnetic behaviour as the non-magnetic $La_3Pt_{23}Si_{11}$ counterpart.

Acknowledgments

We are grateful to S. Pairis for the SEM observations and analysis. We thank also A. Hadj-Azzem, J. Balay, Y. Deschanels, E. Eyraud, D. Dufeu and P. Lachkar for their technical assistance.

References

[1] A. I. Tursina, A. V. Gribanov, Y. D. Seropegin, K. V. Kuyukov, O. I. Bodak, J. Alloys Compd. 347 (1-2) (2002) 121 – 123.

[2] C. Opagiste, C. Paulsen, E. Lhotel, P. Rodiere, R.-M. Galera, P. Bordet, P. Lejay, J. Magn. Magn. Mater. 321 (6) (2009) 613 – 618.

[3] C. Opagiste, R.-M. Galéra, M. Amara, C. Paulsen, S. Rols, B. Ouladdiaf, Phys. Rev. B 84 (2011) 134401–1 – 134401–9.

[4] C. Opagiste, R.-M. Galéra, Journal of Alloys and Compounds 541 (2012) 403 – 406.

[5] C. Opagiste, M. Jackson, R.-M. Galéra, E. Lhotel, C. Paulsen, B. Ouladdiaf, Journal of Magnetism and Magnetic Materials 340 (2013) 46 – 49.

[6] C. Opagiste, R.-M. Galéra, Journal of Magnetism and Magnetic Materials 357 (2014) 13 – 17.

[7] P.-G. de Gennes, C. R. Acad. Sc. 247 (1958) 1836 – 1838.

[8] D. Kaczorowski, A. Gribanov, S. Safronov, P. Rogl, Y. Seropegin, Journal of Alloys and Compounds 509 (37) (2011) 8987 – 8990.

[9] C. M. Varma, Rev. Mod. Phys. 48 (1976) 219–238.

[10] J. M. Lawrence, P. S. Riseborough, R. D. Parks, Reports on Progress in Physics 44 (1) (1981) 1–84.

[11] N. Tsujii, H. Kontani, K. Yoshimura, Phys. Rev. Lett. 94 (2005) 134401.

[12] J. Flouquet, D. Aoki, F. Bourdarot, F. Hardy, E. Hassinger, G. Knebel, T. D. Matsuda, C. Meingast, C. Paulsen, V. Taufour, Journal of Physics: Conference Series 273 (2011) 012001 – 012025.

[13] N. M. Voronov, Izv. Sekt. Platiny 13 (1936) 145 – 166.

[14] J. Rodriguez-Carvajal, Satellite Meeting on Powder Diffraction of the XV Congress of the IUCr, Book of Abstracts, 1990.

[15] A. Arrott, Phys. Rev. 108 (1957) 1394 – 1396.

[16] K. H. J. Buschow, A. M. van Diepen, H. W. de Wijn, Phys. Rev. B 8 (1973) 5134–5138.

[17] A. Kramida, Yu. Ralchenko, J. Reader, and NIST ASD Team, NIST Atomic Spectra Database (ver. 5.2), [Online]. Available: `http://physics.nist.gov/asd` [2014, September 24]. National Institute of Standards and Technology, Gaithersburg, MD. (2014).

[18] A. Frank, Phys. Rev. 39 (1932) 119 – 129.